

Dynamics of the superconducting order parameter through ultrafast normal-to-superconducting phase transition in $\text{Bi}_2\text{Sr}_2\text{CaCu}_2\text{O}_{8+\delta}$ from multi-pulse polarization-resolved transient optical reflectivity

I. Madan,^{1,2} V.V. Baranov,¹ Y. Toda,³ M. Oda,⁴ T. Kurosawa,⁴ V.V. Kabanov,¹ T. Mertelj,^{1,5,*} and D. Mihailovic^{1,5}

¹Complex Matter Department, Jozef Stefan Institute, Jamova 39, 1000 Ljubljana, Slovenia

²Laboratory for Ultrafast Microscopy and Electron Scattering, IPHYs, École Polytechnique Fédérale de Lausanne, CH-1015 Lausanne, Switzerland

³Department of Applied Physics, Hokkaido University, Sapporo 060-8628, Japan

⁴Department of Physics, Hokkaido University, Sapporo 060-0810, Japan

⁵Center of Excellence on Nanoscience and Nanotechnology Nanocenter (CENN Nanocenter), Jamova 39, 1000 Ljubljana, Slovenia

A systematic temperature dependent study of the femtosecond optical superconducting (SC) state destruction and recovery in $\text{Bi}_2\text{Sr}_2\text{CaCu}_2\text{O}_{8+\delta}$ cuprate superconductor by means of the all-optical polarization-sensitive multi-pulse spectroscopy is presented. At low temperatures and a partial SC state suppression an anisotropic SC-gap recovery-timescale is suggested by the data. The SC state destruction and recovery dynamics are compared to the recent TR-ARPES-inferred SC-gap dynamics and a qualitative agreement is found. Using a phenomenological response function the experimental data are also compared to time dependent Ginzburg-Landau model simulations.

I. INTRODUCTION

The study of the time evolution of complex systems through symmetry breaking transitions (SBT) is of great fundamental interest in different areas of physics^{1–3}. An SBT of particular general interest is the ultrafast normal-to-superconducting (N→S) state transition. Due to the small heat capacity of the electronic system, an optical pulse can efficiently suppress the SC state without heating the low-frequency phonon heat bath, which remains well below the critical temperature (T_c). This enables us to perform an ultrafast effective⁴ electron temperature quench across T_c with an ultrashort laser pulse, which is then followed by an ultrafast non-equilibrium N→S transition.

The ultrafast S→N→S transition in the cuprate superconductors has been initially studied by all-optical^{5–9} pump-probe technique followed by laser ARPES^{10–13}. While the laser ARPES can directly resolve the momentum dependent¹⁴ quasiparticle (QP) distribution function, all-optical techniques offer better bulk sensitivity and greater flexibility. The lack of momentum resolution of an optical probe can be partially compensated by use of the optical dipole transition selection rules that depend on the probe-photon polarization^{15,16} and energy^{8,17} and enable selection of different parts of the Brillouin zone (BZ).

The electronic Raman-scattering tensor analyses have shown¹⁵ that the dielectric tensor fluctuations of different symmetries can be linked to charge excitations in different parts of the BZ. In particular, in a D_{4h} point-symmetry corresponding to the ideal CuO_2 -plane symmetry, the dielectric tensor fluctuations with the B_{1g} and B_{2g} symmetries are linked to the anti-nodal and nodal BZ charge excitations, respectively, while the totally symmetric A_{1g} fluctuations do not discriminate between the regions. The transient reflectivity, ΔR , is related to the

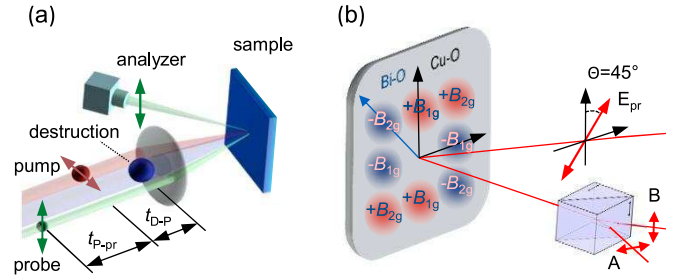


Figure 1. (a) Schematic representation of the three-pulse experiment and notation of delays between pulses. (b) Schematic representation of the detection of $\Delta R_{B_{1g}}$ using a Wollaston prism. The initial probe polarization is set at 45° with respect to the Cu-O bond direction. The intensity in channels A and B is balanced and the differential signal is recorded, so that all contributions except $\Delta R_{B_{1g}}$ are canceled out.

Raman tensor and in $\text{Bi}_2\text{Sr}_2\text{CaCu}_2\text{O}_{8+\delta}$ (Bi2212) the B_{1g} -like¹⁸ transient reflectivity component shows sensitivity to the SC state only, while A_{1g} -like and B_{2g} -like transient reflectivity components couple to both the SC and pseudogap (PG) order.¹⁶

While the all-optical transient response in the cuprates under weak excitation can be well described in terms of the photoinduced absorption of the photoexcited quasiparticles¹⁹ the response function in highly nonequilibrium states is unclear due to unknown relative contributions of collective and single-particle degrees of freedom to the transient optical reflectivity. To overcome this problem the standard two-pulse all-optical pump-probe technique was extended to a multi-pulse technique, which was shown to be instrumental in extracting the order parameter dynamics in a charge density wave compound²⁰ as well as in the prototypical cuprate superconductor

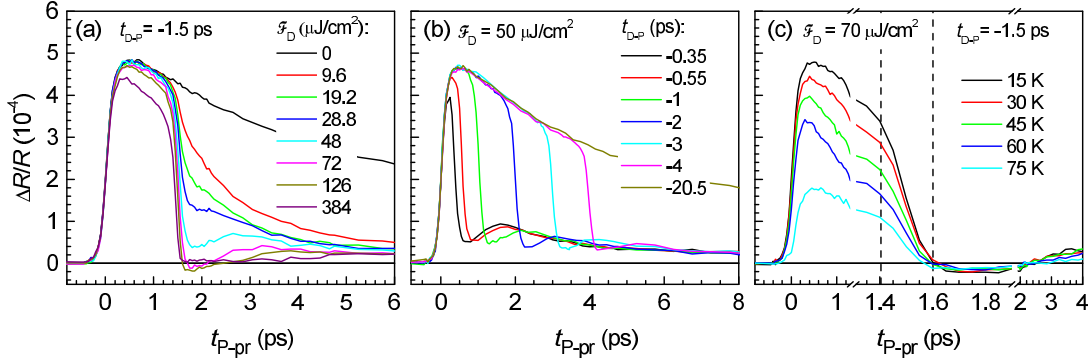


Figure 2. The influence of the destruction pulse on the transient reflectivity in the superconducting state, when the D pulse arrives after the P pulse using the PDS. (a) and (b) show dependence on the D-pulse fluence and t_{D-P} delay at $T = 15$ K, respectively. (c) T -dependence of the transient reflectivity suppression.

$\text{La}_{1.9}\text{Sr}_{0.1}\text{CuO}_4$ ²¹.

Here we extend our previous study²¹ of an ultrafast $S \rightarrow N \rightarrow S$ transition in $\text{La}_{1.9}\text{Sr}_{0.1}\text{CuO}_4$ to $\text{Bi}_2\text{Sr}_2\text{CaCu}_2\text{O}_{8+\delta}$ in search of universality, and also to uncover potential important differences in the two materials with substantially different critical temperatures and pseudogap/SC gap ratios. By means of the all-optical multi-pulse technique combined with the polarization selective optical probe we were able to separate the SC state recovery dynamics from the previously studied²² PG state recovery dynamic and enable discrimination between relaxation in the nodal and anti-nodal BZ regions. The material has been studied previously by time-resolved techniques^{7,8,10–12,23}, but thus far there has been no systematic study of the non-equilibrium transitions in this material, especially by the 3-pulse technique.

While we found that in $\text{La}_{1.9}\text{Sr}_{0.1}\text{CuO}_4$ the time dependent Ginzburg-Landau (TDGL) theory can provide a fair quantitative description of the SC order parameter recovery, only a qualitative description of the data is possible in $\text{Bi}2212$, which we attribute to the large SC order fluctuations in the PG state near time of the transition. In addition, when only a partial SC state suppression is achieved, the polarization resolved optical probe enables us to detect anisotropic SC-order recovery timescales, revealing a faster SC gap recovery in the anti-nodal direction in comparison with the nodal BZ regions.

II. EXPERIMENTAL

The sample used in this work was underdoped $\text{Bi}_2\text{Sr}_2\text{CaCu}_2\text{O}_{8+\delta}$ ($\text{Bi}2212$) single crystal with $T_c \approx 78$ K ($\delta = 0.14$) grown by means of the traveling solvent floating zone method. Before mounting into a liquid-He flow cryostat the sample was freshly cleaved using sticky tape.

The pulse train from a 250-KHz 1.55-eV Ti:Sapphire regenerative amplifier was split into 50 fs destruction (D), pump (P) and probe (pr) pulse trains that were independently delayed with respect to each other. The result-

ing beams were focused and overlapped on the sample [see Fig. 1 (a)]. As in the standard pump-probe spectroscopic experiments the transient reflectivity $\Delta R/R$ was measured by monitoring the intensity of the weakest pr beam. The direct contribution of the unchopped D beam to ΔR was rejected by means of a lock-in synchronized to the chopper that modulated the intensity of the P beam only. The fluences $\mathcal{F}_P < 5 \mu\text{J}/\text{cm}^2$ and $\mathcal{F}_{pr} < 3 \mu\text{J}/\text{cm}^2$ of the P and pr pulses were kept in the linear response region, well below the superconductivity destruction threshold^{7,8,24}.

To select different components of the anisotropic transient reflectivity¹⁶ two different polarization sensitive detection schemes were used. In the parallel detection scheme (PDS), which is sensitive to the sum of $\Delta R_{A_{1g}}$ and $\Delta R_{B_{1g}}$ components²⁵, $\Delta R = \Delta R_{A_g} + \Delta R_{B_{1g}}$, we used a single photodiode detection with an analyzer parallel to the pr-beam polarization, where the pr-beam polarization was parallel to the Cu-O bond direction. The polarizations of the P and D beams were perpendicular to the pr-beam polarization in order to suppress the signal due to P beam scattering.

In the balanced detection scheme (BDS), which is sensitive to the $\Delta R_{B_{1g}}$ component only, the pr-beam polarization was oriented at 45° with respect to the Cu-O bond directions and two photodiodes in combination with a Wollaston prism were used for detection [see Fig. 1 (b)]. When the polarization axes of such detector are oriented along the Cu-O bond directions, the difference of the two photodiode photocurrents corresponds to $\Delta R_{B_{1g}}$, while $\Delta R_{A_{1g}}$ and $\Delta R_{B_{2g}}$ components are rejected. Fine alignment of the polarization and detector angles was done in the PG state at 120 K, to achieve a complete cancellation of the transient PG response.

In order to suppress the P beam scattering contribution to the signal in the BDS the P-beam frequency was doubled (3.1-eV P-photon energy) and a long-pass filter in front of the detector was used while the 1.55-eV D-photon energy was the same as in the first scheme.²⁶

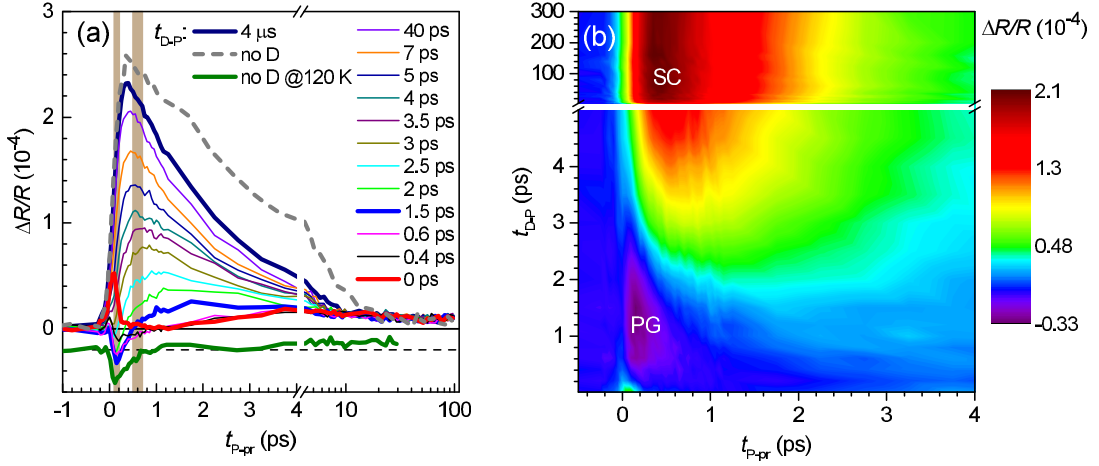


Figure 3. (a) Transient reflectivity using the PDS at $T = 40$ K with $\mathcal{F}_D = 68 \mu\text{J}/\text{cm}^2$. For comparison a transient measured in the PG state ($T = 120$ K) in the absence of the D pulse is shown vertically shifted below the main data. The vertical shaded areas indicates the read-out t_{P-pr} delays (see text). (b) The same data set as in (a) shown as a colormap. At $t_{D-P} = 0$ both the PG and SC signal are suppressed. With increasing t_{D-P} one can observe a sequential recovery of the negative PG response followed by the positive SC response.

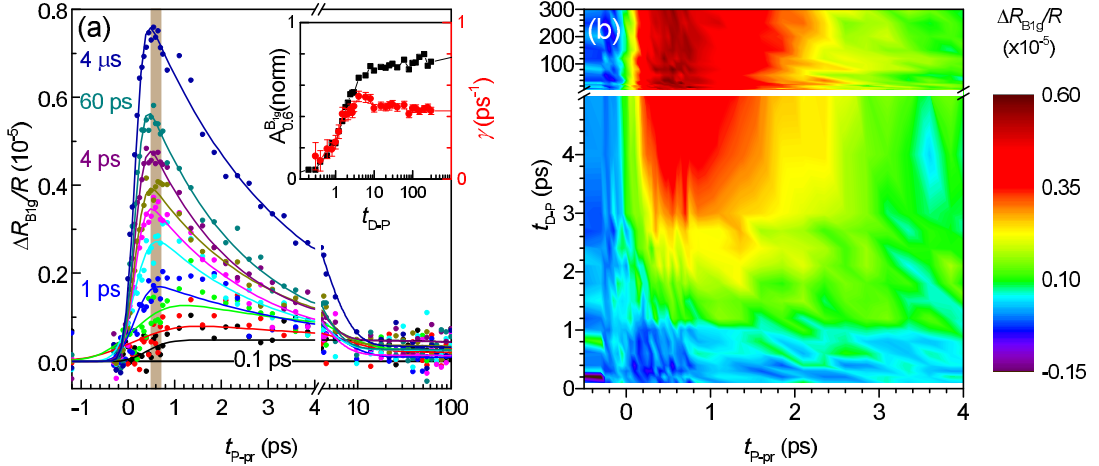


Figure 4. (a) Recovery of the transient-reflectivity B_{1g} component at $T = 40$ K and $\mathcal{F}_D = 56 \mu\text{J}/\text{cm}^2$. The vertical shaded area represents the interval used to determine A_{SC} . Inset: black squares (left axis) - normalized amplitude of the response, red circles - relaxation rate extracted from single-exponential fits to the traces. Error bars are the standard errors of the regression analysis. (b) The same data as in (a) shown as a color map in $t_{D-P} - t_{P-pr}$. In the absence of the PG response recovery of the SC signal is evident already at $t_{D-P} \sim 1$ ps.

III. RESULTS

A. SC state destruction

To illustrate the destruction of the SC state, in Fig. 2 we plot the transient reflectivity for the case when the D pulse arrives after the P pulse using the PDS. Depending on the D pulse fluence, \mathcal{F}_D , the transient reflectivity is suppressed to different degrees. Above $\mathcal{F}_D \sim 70 \mu\text{J}/\text{cm}^2$, SC order is completely suppressed on a 200-fs timescale after the D-pulse arrival. Above $\mathcal{F}_D \sim 70 \mu\text{J}/\text{cm}^2$ we observe also a small negative overshoot lasting a few hundred femtoseconds followed by a weak recovery of the signal on

a picosecond timescale. Both features vanish at the highest fluence of $\sim 400 \mu\text{J}/\text{cm}^2$. The suppression timescale does not depend on the D-pulse arrival time [Fig. 2 (b)] nor temperature [Fig. 2 (c)].

B. SC state recovery

In Fig. 3 we show a typical transient reflectivity data set measured in the PDS for the case when the P pulse arrives after the D pulse. After a complete suppression for $t_{D-P} \lesssim 0.5$ ps we first observe a recovery of the negative PG component on a 1 \sim ps timescale followed by the

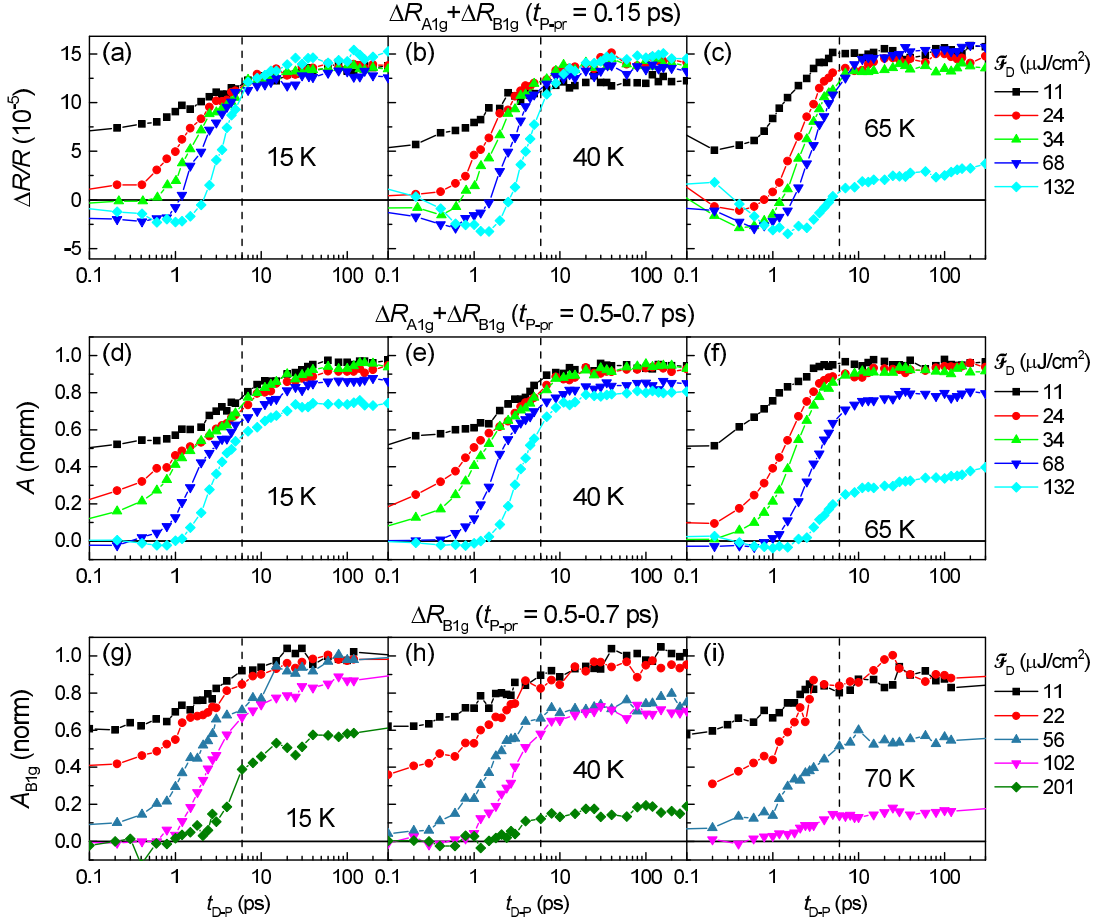


Figure 5. (a)-(c) The transient reflectivity at $t_{P-pr} = 0.15$ ps, corresponding to the delay at which the PG response peaks, as a function of t_{D-P} for different D-pulse fluences at different temperatures. (d)-(f) Evolution of the normalized $\Delta R/R$ amplitude averaged in the $0.5 \text{ ps} \leq t_{P-pr} \leq 0.7 \text{ ps}$ range as a function of t_{D-P} for different D-pulse fluences at different temperatures. (g)-(i) the same for $\Delta R_{B1g}/R$.

recovery of the positive SC component.

As shown previously¹⁶ the PG response does not contribute to ΔR_{B1g} so recovery of the SC component on the short t_{D-P} timescale can be observed more clearly in the BDS. In Fig. 4 we show a typical transient reflectivity data set measured using the BDS. As expected, the PG component is suppressed, but the signal-to-noise ratio is reduced due to a smaller ΔR_{B1g} amplitude.

IV. ANALYSIS AND DISCUSSION

A. SC state destruction

The destruction timescale of ~ 200 fs is T and \mathcal{F} independent and faster than ~ 700 fs in LSCO^{6,9}. In LSCO it was suggested^{6,9} that the high energy optical phonons created during the relaxation of the primary photo electron-hole pair are the dominating pair breaking excitation setting the destruction timescale.

The faster destruction timescale in Bi2212 does not

exclude the same phonon mediated destruction mechanism since one polar optical phonon can be generated by a photoexcited electron/hole every ~ 5 fs⁹. Taking the initial photo electron/hole energy of ~ 1 eV and optical phonon energy of 50 meV leads to ~ 100 fs photo electron/hole energy relaxation time that is fast enough to be compatible with the experimental data²⁷. The phonon dominated pair-breaking destruction of the SC state is supported also by the large optical SC state destruction energy that is 5 times larger than the SC condensation energy.²⁴

B. Analysis of the SC state recovery

To analyze the recovery we first fit a finite-rise-time single-exponential relaxation model to the transient reflectivity in Fig. 4 to obtain the t_{D-P} dependent relaxation rate γ . In the inset to Fig. 4 (a) we compare the relaxation rate γ from the fit to the amplitude of the B_{1g} SC response $A_{B1g} = \Delta R_{B1g}/\Delta R_{B1g, \text{no-D}}$,

where \bar{y} corresponds to the average of y in the interval²⁸ $t_{P-pr} = 0.5 - 0.7$ ps and $\Delta R_{B_{1g}, no-D}$ to the transient reflectivity in the absence of the D pulse.

γ and $A_{B_{1g}}$ initially recover on a similar time-scale of ~ 4 ps followed by slower dynamics extending towards the nanosecond timescale. As in the case of (La,Sr)CuO_{4+ δ} (LSCO), we attribute the suppression of γ during the first part of the recovery to the critical slowing down of the SC fluctuations in the vicinity of the transition.²¹ Upon the initial increase γ decreases on the nanosecond timescale indicating cooling of the probed volume: Since the effective temperature on longer timescales is far from the critical temperature the T -dependence of γ is no longer critical but determined by the Rothwarf-Taylor bottleneck dynamics.²⁹

Contrary to LSCO, where the PG component shows no suppression up to a rather high excitation fluence,³⁰ the PG component in Bi2212 shows suppression already below²² $\sim 100 \mu\text{J}/\text{cm}^2$ so also the PG component is affected by the D pulse. To extract the SC component recovery dynamics in the PDS it is therefore necessary to take the PG dynamics into account.

The PG component peaks at $t_{D-pr} = 0.15$ ps. Traces of $\Delta R/R$ at this t_{D-pr} as function of t_{D-P} are shown in Fig. 5 (a-c). It is evident that at higher \mathcal{F}_D the PG recovery leads to non-monotonous traces due to the sub-ps recovery timescale²² of the negative PG component preceding the recovery of the positive SC-state component. Due to the rather fast PG-component relaxation time¹⁶ [see Fig. 3 (a)] the contribution of the PG component to $\Delta R/R$ should diminish with increasing t_{D-pr} . Taking t_{P-pr} in the interval $0.5 \text{ ps} < t_{P-pr} < 0.7 \text{ ps}$ where $\Delta R_{B_{1g}}/R$ has a peak³¹ in the absence of the D pulse and the PG response is already suppressed, we calculate the normalized average, $A = \overline{\Delta R}/\overline{\Delta R_{no-D}}$. Indeed, $A(t_{D-P})$ traces presented in Fig. 5 (d-f) show significantly less PG-component recovery and appear very similar to the equivalent $A_{B_{1g}}(t_{D-P})$ traces shown in Fig. 5 (g-i).

At $T > T_c$ the PG recovers on the ~ 0.7 ps timescale²². To check whether the amplitude of the PG component is modified during the slower SC state recovery¹⁷ we compare in Fig. 6 the two readouts with different PG contribution taken at $t_{P-pr} = 0.15$ ps and the average in the interval $0.5 \text{ ps} < t_{P-pr} < 0.7 \text{ ps}$ (A). At the highest $\mathcal{F}_D = 132 \mu\text{J}/\text{cm}^2$ it is possible to overlap the traces beyond $t_{D-pr} \gtrsim 1$ ps at all measured temperatures when plot as a function of³² t_{D-pr} by vertically shifting³³ and rescaling. At intermediate \mathcal{F}_D s the complete overlap is not possible. The shifted and rescaled readouts at $t_{P-pr} = 0.15$ ps show slightly higher values in the $\sim 2 - \sim 10$ -ps delay range. This could indicate that the negative PG response at 1.55-eV probe-photon energy is transiently suppressed³⁴ by the appearance of the SC order.

A possibly related suppression of the PG component in the SC state at 1.08-eV probe-photon energy was suggested recently¹⁷. Considering an earlier report⁸, however, where by selecting a particular polarization and

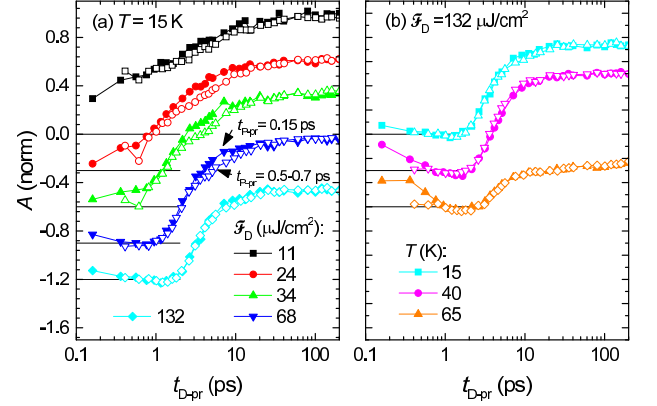


Figure 6. Comparison of A_S at two different t_{P-pr} as a function of t_{D-pr} . The traces are vertically shifted for clarity as indicated by the horizontal thin lines. Full and open symbols correspond to $t_{P-pr} = 0.15$ ps and $t_{P-pr} = 0.5 - 0.7$ ps, respectively. The strongly PG-affected ($t_{P-pr} = 0.15$ ps) traces (full symbols) are vertically shifted and scaled to achieve the best match for $t_{D-pr} \gtrsim 1$ ps.

probe-photon energy no suppression of the PG component in the SC state was observed, we attribute the difference between readouts in our experiment to the SC-gap dependent pre-bottleneck SC-state dynamics, which influences the readouts at $t_{D-P} = 0.15$ ps.

C. SC state recovery timescale in nodal and anti-nodal response

In Fig. 7 (b) we compare the fluence dependencies of the SC recovery time, τ_{rec} , for both symmetries to the standard 2-pulse transient-reflectivity relaxation time, τ_{2p} . We estimate τ_{rec} using a phenomenological exponential fit:

$$A_S = A_T - A_e e^{-t_{D-P}/\tau_{rec}}, \quad (1)$$

to the trajectories in Fig. 5(d)-(i). The lower \mathcal{F}_D data can be rather well fit using the simple single-exponential recovery model (1) while at higher \mathcal{F}_D the recovery appears clearly non exponential as shown in Fig 7 (a).

As a function of fluence both, τ_{rec} and τ_{2p} show a minimum at intermediate fluences. Above $\mathcal{F}_D \sim 100 \mu\text{J}/\text{cm}^2$ timescales of different signals match rather well³⁶ and show virtually no T -dependence [see Fig. 7 (c)]. At low \mathcal{F}_D and $T = 15$ K, however, the A_{1g} -dominated-channel τ_{rec} slows down much more with decreasing \mathcal{F}_D than the B_{1g} -channel τ_{rec} and τ_{2p} . On the contrary, at $T = 40$ K, both, the A_{1g} -dominated- and B_{1g} -channel τ_{rec} show identical fluence dependence in the full \mathcal{F}_D range with a sharp up-turn at $\mathcal{F}_D \sim 60 \mu\text{J}/\text{cm}^2$.

A faster $\Delta R/R$ relaxation in the B_{1g} configuration has been observed already in the low excitation 2-pulse

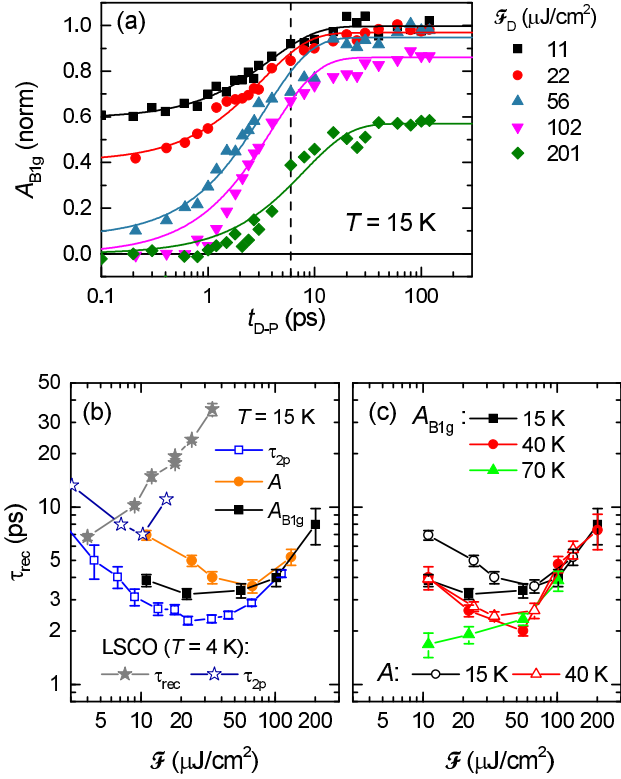


Figure 7. (a) Fits of Eq. (1) to the A_{B1g} trajectories at $T = 15$ K. (b) The recovery time of the superconducting response from the fits at $T = 15$ K as a function of fluence for A_{B1g} and A trajectories [Fig. 5 (d) and (g)]. For comparison the $\Delta R/R$ relaxation time from a two-pulse experiment at 15 K in Bi2212 is shown by open squares. The corresponding relaxation times in LSCO³⁵ at $T = 4$ K are shown by stars. (c) Temperature dependence of τ_{rec} of A_{B1g} (full symbols) and A (open symbols) trajectories.

experiments.¹⁶ Due to the sensitivity of the the B_{1g} configuration to the anti-nodal Brillouin-zone (BZ) region this is consistent with a faster quasiparticle relaxation around anti-nodes³⁷ either by recombination or by scattering into the nodal BZ region, which contributes to the A_{1g} -dominated channel showing a slower decay.

The effect of the faster antinodal quasiparticle relaxation is also evident in our 3-pulse experiment, but only, when the SC order is not completely suppressed and T is below ~ 40 K. From the 3-pulse data it appears that upon a modest suppression the SC gap recovers faster at the anti-nodes than near the nodes.

At higher \mathcal{F}_D upon a complete suppression of the SC gap our data suggest the recovery that is more homogeneous across the Fermi surface. This could be attributed to two factors. First, during the initial part of the recovery the suppression of the Rothwarf-Taylor phonon bottleneck²⁹ and lifting of the SC-gap-imposed QP-relaxation phase space restrictions³⁸ enable efficient transfer of the excess QP energy to the phonon bath together with efficient diffusion of excitations across all of the BZ. Second, at higher \mathcal{F}_D the lattice bath is heated

closer to T_c so the QP-relaxation phase space restrictions can be easier overcome by the phonon assisted QP scattering.

In LSCO [Fig. 7 (b)] τ_{rec} is similarly to τ_{2p} significantly longer than in Bi2212.⁸ The generally slower τ_{2p} and τ_{rec} in LSCO could be attributed to the smaller SC gap enhancing the quasiparticle relaxation bottleneck¹⁹. Moreover, in LSCO τ_{rec} increases monotonically above the destruction threshold fluence,⁶ $\mathcal{F}_{Dth} = 4.2 \mu\text{J}/\text{cm}^2$, while in Bi2212 with⁸ $\mathcal{F}_{Dth} = \sim 16 \mu\text{J}/\text{cm}^2$, the increase starts only above $\sim 4\mathcal{F}_{Dth}$. This could be attributed to the lattice temperature after the quench being closer³⁹ to T_c in LSCO than in Bi2212 resulting in a stronger critical slowing down of the SC order parameter dynamics.

D. Time dependent Ginzburg-Landau model

We proceed by analyzing the trajectory of the SC amplitude through the transition in the framework of the time-dependent Ginzburg-Landau (TDGL) theory. In previous study²¹ of the SC-order recovery in LSCO we have shown that the TDGL theory fails to consistently describe the ultrafast optical destruction of the SC condensate. On the other hand, *the SC condensate recovery can be quantitatively modeled* using a phenomenological response function and the Ginzburg-Landau time, τ_{GL} , as the only free fit parameter assuming a finite magnitude of the initial depth-dependent order parameter (Fig. 3c in Ref. [21]). The magnitude of the initial order parameter corresponds to the magnitude of the frozen SC fluctuations after the quench from the normal/PG to the SC state which is a function of the depth-dependent quench-rate (Eq. (4) in Ref. [21]). In LSCO even better fit is possible using a phenomenological depth-dependent initial order parameter $\psi_{BC}(z)$:

$$\psi_{BC}(z) = \begin{cases} cz & ; U_D(z) > U_{th} \\ \sqrt{1 - T/T_c} & ; U_D(z) \leq U_{th}, \end{cases} \quad (2)$$

where c is an additional \mathcal{F}_D -dependent free parameter, $U_D(z)$ the depth-dependent absorbed optical-energy density and U_{th} the SC-destruction-threshold optical-energy density.

In the following we apply a similar TDGL approach to the SC state recovery dynamics in Bi2212.

1. Response function

As a starting point one needs to establish the relation between the superconducting order parameter magnitude, $|\psi_{GL}|$, and the transient optical response amplitude. This relation was in the case of LSCO established phenomenologically from the temperature dependence of the normalized weak-excitation $\Delta R/R$ amplitude, A_S .

In Bi2212 A_S does not go to zero at T_c due to the large pairing fluctuations^{40,41} above T_c as shown in Fig. 8

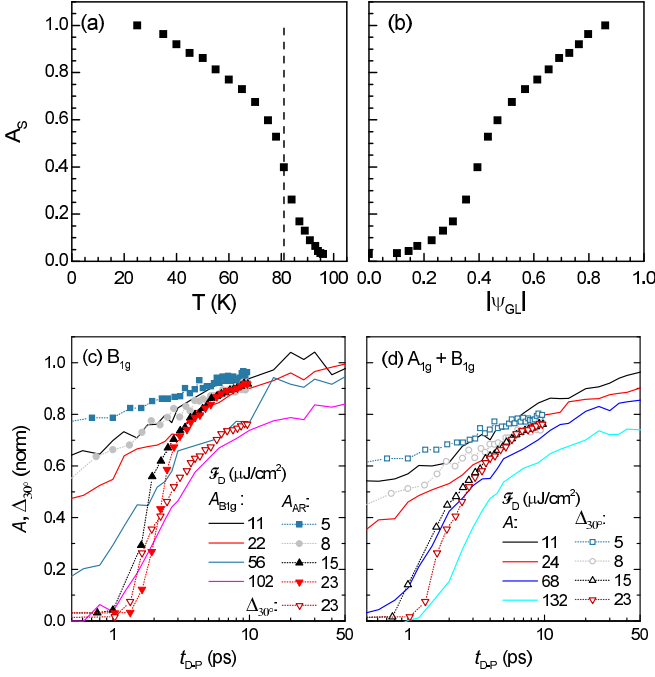


Figure 8. (a) The amplitude of the normalized transient superconducting response as a function of temperature. The dashed vertical line marks the critical temperature measured by a SQUID magnetometer. (b) The amplitude of the the normalized transient superconducting response as a phenomenological function of the GL order parameter obtained from (a) assuming a mean-field $T_c^{MF} = 96$ K. This relation is used as the response function for the theoretical calculation of the superconducting order parameter evolution presented in Fig. 9. (c) Comparison of A_{B1g} to A_{AR} obtained from the TR-ARPES gap dynamics¹¹ using the response function from (b). The normalized TR-ARPES gap (open symbols) at the highest \mathcal{F}_{ARPES} is also shown for comparison. (d) Comparison of $A_{0.6}$ to the normalized TR-ARPES gap.

(a), inconsistently with the the GL theory. However, by taking into account that A_S is sensitive to the pairing amplitude⁴¹ and not the SC phase coherence, we can still apply the GL description assuming that only the SC phase coherence is established at T_c , while the largest temperature at which A_S is still observable corresponds to the mean-field pairing critical temperature, $T_c^{MF} \simeq 96$ K. Implying the standard GL T -dependence of the (pairing) order parameter, $\psi_{GL} \propto \sqrt{1 - T/T_c^{MF}}$, we can now establish the response function as shown in Fig. 8(b).

To further analyze the link between the SC order parameter and A_S we compare our results to recent TR-ARPES gap dynamics data in near-optimally doped Bi2212 ($T_c = 91$ K).¹¹ Considering the different doping levels of the samples and different spatial⁴² and reciprocal-space⁴³ sensitivity of the probes only a qualitative correspondence between the results is expected, since even in the case of TR-ARPES the extraction of the SC gap is not rigorously defined¹¹. For the sake of comparison we therefore assume that $|\psi_{GL}(t)| \propto \Delta_{30^\circ}(t)$,

where $\Delta_{30^\circ}(t)$ corresponds to the TR-ARPES gap at the edge of the Fermi arc and calculate $A_{AR}(t)$ using the response function in Fig. 8(b). In Fig. 8 (c) and (d) we show comparison of our data to both, A_{AR} and the TR-ARPES gap, Δ_{30° .

For the B_{1g} configuration we find a surprisingly good match between A_{AR} and A_{B1g} in the low fluence⁴⁴ region, where the SC gap is only partially suppressed. At higher \mathcal{F} , where the gap⁴⁵ is completely suppressed, the dynamics appears significantly different below ~ 3 ps, unless we compare curves with very different fluences. Ignoring the response function a direct comparison of Δ_{30° at $\mathcal{F} = 23 \mu J/cm^2$ to A_{B1g} at 4.4 times higher $\mathcal{F} = 102 \mu J/cm^2$ gives a good match in the region of the strong suppression of the gap.

For the A_{1g} dominated configuration a better match is observed when we compare A to Δ_{30° directly [Fig. 8 (d)] while A_{AR} shows consistently higher magnitude than A . Similarly to the B_{1g} configuration, a good match is observed at a complete SC gap suppression between the TR-ARPES trajectory at $\mathcal{F} = 15 \mu J/cm^2$ and A at 4.5 times higher $\mathcal{F} = 68 \mu J/cm^2$.

Assuming that the TR-ARPES SC gap dynamics is *identical to the bulk gap* dynamics the difference between the fluences of the corresponding-timescales data can be, at least partially⁴⁴, attributed to the smearing of the optical-probe dynamics due to the depth-dependent excitation density and SC gap suppression. This is corroborated by the convergence of the optical and TR-ARPES trajectories with similar fluence on longer timescales, when the spatial inhomogeneity is expected to decrease.

The inaccuracy of the empirical response function [Fig. 8 (b)] can further contribute to the difference, especially in the region of small SC order parameter. Contrary to LSCO²¹ where the response function is linear up to $A_S \sim 0.8$ the s-shape of the response function in the present case suggests that A_{AR} might be underestimated for low values of the gap.

Importantly, taking into account the inherent differences between the techniques we can conclude that the TR-ARPES Fermi-arc SC gap and the antinodal SC gap inferred from the B_{1g} channel multi-pulse optical probe show qualitatively identical suppression and recovery dynamics.

2. Simulations

As in the case of LSCO²¹ we simulate the evolution of the order parameter through the transition by solving the dimensionless form of the first of the two TDGL equations:

$$\frac{\partial \psi}{\partial t} = \alpha_r(t, z)\psi - \psi|\psi|^2 + \nabla^2 \psi, \quad (3)$$

where time and length are measured in units of τ_{GL} (fit parameter) and the coherence length, respectively.

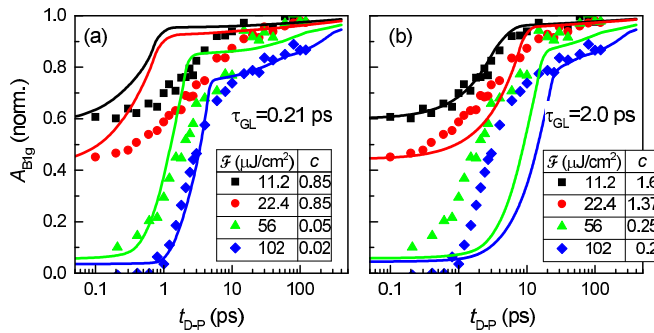


Figure 9. Comparison of the simulated amplitude of the transient superconducting response to the B_{1g} experimental data measured at 15 K. (a) and (b) correspond to different values of τ_{GL} indicated in the graphs. Tables show the values of the parameter c defining the initial order parameter [Eq. (2)].

$\alpha_r(t, z)$ is a time- and depth-dependent reduced temperature which is the solution of the three temperature model²⁷ combined with the heat diffusion equation.²¹

We neglect the second TDGL equation and any lateral variation of the order parameter, assuming that all the Kibble-Zurek (KZ) physics^{46,47} can be phenomenologically absorbed into the initial order parameter $\psi_{BC}(z)$ using (2), and the phase dynamics, i.e. the dynamics of vortices, does not significantly modify the order parameter amplitude.

The two fitting parameters c and τ_{GL} are rather independent. While the first defines the Kibble-Zurek-physics-related amplitude of the response at $t = 0$, the second defines the time-scale of the recovery. In Fig. 9 we present typical results of the simulations for two different values of the τ_{GL} optimized to fit the highest- \mathcal{F}_D and the lowest- \mathcal{F}_D trajectories at 15 K, respectively. One can see that while a decent agreement for a targeted curve can be achieved, one needs to significantly vary τ_{GL} to fit the complete data set. Since such variation is unphysical, we can state that the presented TDGL approach is only sufficient to describe the present data qualitatively, contrary to what was found in LSCO, where a more quantitative description is possible.

The lack of quantitative description can not be attributed to the omission of the second TDGL equation and the resulting vortex dynamics it describes. While at a partial SC-state order parameter suppression no KZ-vortices formation is expected more vortices would be created with further suppression. The presence of vortices at increased order parameter suppression is expected to further slow down the SC-state recovery⁴⁸. Looking at Fig. 9 one can clearly see, that even without the vortex dynamics the TDGL solutions display a stronger recovery-timescale slowdown with increased order parameter suppression than the experimental data, so inclusion of the vortex dynamics into modeling is ex-

pected to only increase the discrepancy.

On the other hand, the lack of quantitative description is not very surprising due to the large pairing fluctuations contribution⁴¹ to the transient reflectivity above T_c that prevents strict applicability of the TDGL theory and undermine the phenomenological link between the order parameter magnitude and the experimentally observable A_s .

V. SUMMARY AND CONCLUSIONS

Our systematic investigation of the ultrafast optical suppression and recovery of the superconducting state in $Bi_2Sr_2CaCu_2O_{8+\delta}$ by means of polarization-selective multi-pulse optical time-resolved spectroscopy leads to some interesting, and somewhat surprising new findings. We found that the SC order is suppressed on the 200-fs timescale, comparable to the recent laser TR-ARPES¹¹ results. The destruction timescale is independent of the temperature and optical destruction pulse energy and is consistent with a photoexcited carrier energy-transfer to the high-energy pair breaking phonons.

The recovery of the SC order is slower appearing on the 2-8 ps timescale showing non-monotonous dependence on the destruction pulse energy. At low T and a partial SC-state suppression the data shows that the SC gap in the antinodal region recovers faster than near the nodes. Perhaps surprisingly, the recovery also slows down with decreasing T highlighting the importance of thermal fluctuations in the recovery mechanism. When the SC state is strongly suppressed, the recovery becomes non-exponential with the recovery timescale slowing down, becoming T -independent.

The fact that the antinodal SC order parameter recovery dynamics inferred from the B_{1g} channel and the TR-ARPES Fermi-arc SC gap dynamics¹¹ show qualitatively identical recovery dynamics gives us confidence in the significance of the multipulse technique.

Despite strong SC fluctuations above T_c and the anisotropic SC-gap recovery the time dependent Ginzburg-Landau model qualitatively describes the SC-order temporal dynamics reasonably well, considering its limitations.

ACKNOWLEDGMENTS

The authors acknowledge the financial support of Slovenian Research Agency (research core funding No-P1-0040) and European Research Council Advanced Grant TRAJECTORY (GA 320602) for financial support. We would like to thank L. Stojchevska for helping with the measurements.

- * tomaz.mertelj@ijs.si
- ¹ Y. M. Bunkov and H. Godfrin, *Topological Defects and the Non-Equilibrium Dynamics of Synthetic Cryogenic Liquids*, edited by Y. M. Bunkov and H. Godfrin (Springer Netherlands, Dordrecht, 2000) p. 396.
 - ² P. W. Higgs, *Physical Review* **145**, 1156 (1966).
 - ³ G. Volovik, *Contemporary Physics*, 5 (Oxford university press, 2010) pp. 451–452.
 - ⁴ The quasiparticle energy distribution is nonthermal so strictly speaking the electronic T is not well defined.
 - ⁵ M. Carnahan, R. Kaindl, J. Orenstein, D. Chemla, S. Oh, and J. Eckstein, *Physica C: Superconductivity* **408**, 729 (2004).
 - ⁶ P. Kusar, V. V. Kabanov, J. Demsar, T. Mertelj, S. Sugai, and D. Mihailovic, *Physical Review Letters* **101**, 227001 (2008).
 - ⁷ C. Giannetti, G. Coslovich, F. Cilento, G. Ferrini, H. Eisaki, N. Kaneko, M. Greven, and F. Parmigiani, *Physical Review B* **79**, 224502 (2009).
 - ⁸ Y. Toda, T. Mertelj, P. Kusar, T. Kurosawa, M. Oda, M. Ido, and D. Mihailovic, *Physical Review B* **84**, 174516 (2011).
 - ⁹ M. Beyer, D. Stadtter, M. Beck, H. Schafer, V. V. Kabanov, G. Logvenov, I. Bozovic, G. Koren, and J. Demsar, *Phys. Rev. B* **83**, 214515 (2011).
 - ¹⁰ C. L. Smallwood, J. P. Hinton, C. Jozwiak, W. Zhang, J. D. Koralek, H. Eisaki, D.-H. Lee, J. Orenstein, and A. Lanzara, *Science* **336**, 1137 (2012), <http://science.sciencemag.org/content/336/6085/1137.full.pdf>.
 - ¹¹ C. L. Smallwood, W. Zhang, T. L. Miller, C. Jozwiak, H. Eisaki, D.-H. Lee, and A. Lanzara, *Phys. Rev. B* **89**, 115126 (2014).
 - ¹² C. L. Smallwood, W. Zhang, T. L. Miller, G. Afeldt, K. Kurashima, C. Jozwiak, T. Noji, Y. Koike, H. Eisaki, D.-H. Lee, R. A. Kaindl, and A. Lanzara, *Phys. Rev. B* **92**, 161102 (2015).
 - ¹³ C. Piovera, Z. Zhang, M. d'Astuto, A. Taleb-Ibrahimi, E. Papalazarou, M. Marsi, Z. Z. Li, H. Raffy, and L. Perfetti, *Phys. Rev. B* **91**, 224509 (2015).
 - ¹⁴ Limited to the vicinity to the nodal point on the Γ -Y line.
 - ¹⁵ T. P. Devereaux and R. Hackl, *Reviews of Modern Physics* **79**, 175 (2007).
 - ¹⁶ Y. Toda, F. Kawanokami, T. Kurosawa, M. Oda, I. Madan, T. Mertelj, V. V. Kabanov, and D. Mihailovic, *Physical Review B* **90**, 094513 (2014).
 - ¹⁷ G. Coslovich, C. Giannetti, F. Cilento, S. Dal Conte, T. Abebaw, D. Bossini, G. Ferrini, H. Eisaki, M. Greven, A. Damascelli, and F. Parmigiani, *Phys. Rev. Lett.* **110**, 107003 (2013).
 - ¹⁸ Despite Bi2212 is orthorhombic we use the ideal D_{4h} point group tetragonal CuO_2 -plane symmetry to simplify the notation. See supplemental to Ref. [16] for details.
 - ¹⁹ V. V. Kabanov, J. Demsar, B. Podobnik, and D. Mihailovic, *Phys. Rev. B* **59**, 1497 (1999).
 - ²⁰ R. Yusupov, T. Mertelj, V. V. Kabanov, S. Brazovskii, P. Kusar, J.-H. Chu, I. R. Fisher, and D. Mihailovic, *Nature Physics* **6**, 681 (2010).
 - ²¹ I. Madan, P. Kusar, V. V. Baranov, M. Lu-Dac, V. V. Kabanov, T. Mertelj, and D. Mihailovic, *Physical Review B* **93**, 224520 (2016).
 - ²² I. Madan, T. Kurosawa, Y. Toda, M. Oda, T. Mertelj, and D. Mihailovic, *Nature Communications* **6**, 6958 (2015), arXiv:1410.3205.
 - ²³ P. Kusar, T. Mertelj, V. V. Kabanov, H. Eisaki, M. Wolf, and U. Bovensiepen, *Phys. Rev. Lett.* **107**, 097002 (2011).
 - ²⁴ L. Stojchevska, P. Kusar, T. Mertelj, V. Kabanov, Y. Toda, X. Yao, and D. Mihailovic, *Physical Review B* **84**, 180507 (2011).
 - ²⁵ As in Ref. 16 we use the approximate notation corresponding to the tetragonal symmetry.
 - ²⁶ The scattering from the D-beam does not contribute significantly since the beam is not modulated.
 - ²⁷ L. Perfetti, P. A. Loukakos, M. Lisowski, U. Bovensiepen, H. Eisaki, and M. Wolf, *Phys. Rev. Lett.* **99**, 197001 (2007).
 - ²⁸ In the vicinity of the peak of the unperturbed $\Delta_{R_{B_{1g}}}/R$ -response.
 - ²⁹ V. V. Kabanov, J. Demsar, and D. Mihailovic, *Physical Review Letters* **95**, 147002 (2005).
 - ³⁰ P. Kušar, V. V. Kabanov, S. Sugai, J. Demšar, T. Mertelj, and D. Mihailović, *Journal of superconductivity and novel magnetism* **24**, 421 (2011).
 - ³¹ The $A_{1g} + B_{1g}$ $\Delta R/R$ has a peak at a slightly earlier time, where the PG component contribution is significantly larger.
 - ³² The difference in sampling time of 0.55 ps needs to be taken into account when directly comparing the traces.
 - ³³ The fully recovered PG component contributes to a t_{D-P} -independent negative shift at longer t_{D-P} .
 - ³⁴ When the negative PG component is suppressed the total $\Delta R/R$ increases.
 - ³⁵ P. Kusar, *Influence of Irregularities and Dimensionality on Electron Relaxation*, Ph.D. thesis, Faculty of Mathematics and Physics, University of Ljubljana, Slovenia (2007).
 - ³⁶ Despite the worse fit quality.
 - ³⁷ An consistent increase of the QP relaxation time away from the nodal point was observed in a recent ARPES experiment¹² in some controversy to an earlier ARPES result²³.
 - ³⁸ C. L. Smallwood, T. L. Miller, W. Zhang, R. A. Kaindl, and A. Lanzara, *Phys. Rev. B* **93**, 235107 (2016).
 - ³⁹ In LSCO the lattice temperature after the destruction pulse reaches²¹ T_c at $\mathcal{F}_D = 20 \mu J/cm^2$.
 - ⁴⁰ W. Zhang, C. L. Smallwood, C. Jozwiak, T. L. Miller, Y. Yoshida, H. Eisaki, D.-H. Lee, and A. Lanzara, *Phys. Rev. B* **88**, 245132 (2013).
 - ⁴¹ I. Madan, T. Kurosawa, Y. Toda, M. Oda, T. Mertelj, P. Kusar, and D. Mihailovic, *Scientific Reports* **4**, 5656 (2014).
 - ⁴² The optical penetration depth in Bi2212²⁴ is of the order of 100 nm in comparison to a nm scale photoelectron escape depth.
 - ⁴³ The B_{1g} optical response is sensitive to a broad region near the anti node while the A_{1g} response samples both the nodal and antinodal regions¹⁵.
 - ⁴⁴ Due to the exponential decay of the excitation fluence away from the surface the equivalent external in all-optical experiment is ~ 1.5 times larger than in the case of TR-ARPES.
 - ⁴⁵ The surface gap in the case of TR-ARPES and the bulk gap in the case of optics.
 - ⁴⁶ T. W. B. Kibble and G. E. Volovik,

Journal of Experimental and Theoretical Physics Letters **65**, 102 (1997).
⁴⁸ W. Z. Liu, Physics Reports **276**, 177 (1996).
⁴⁹ Supplemental information to Ref. [21].